3D2-3

Correction of the SCANSAR Scalloping

Masanobu Shimada

Japan Aerospace and Exploration Agency (JAXA), Earth Observation Research Center (EORC), Sengen 2-1-1, Tsukuba, Ibaraki, Japan, 305-8505, Voice 81-29-868-2474, Fax: 81-29-868-2961, shimada.masanobu@jaxa.jp

Abstract SCANSAR is an extra mode of the SAR to widen the swath of STRIP mode in up to several times. PALSAR SCANSAR showed the great performance at the radiometry and geometry and can be fully usable for monitoring the environment, sea ice, wetland, forest, and so on. One of the artifacts that the SCANSAR is sometimes affected is the scalloping, which often appears as duplicated azimuth stripes when the azimuth antenna pattern is not determined accurately. The second artifact is the azimuth ambiguity, which appears over the hetero uniform area when the sampling theorem is not satisfied at the data acquisition. This paper describes a method to determine the azimuth antenna pattern from the SAR data using the Amazon so that the scalloping does not appear, and it also shows a method to select the filter to suppress the azimuth truncation. Some PALSAR sample data corrected shows the proof of the methodology.

I. INTRODUCTION

While the SCANSAR with the wider swath and thus the shorter revisit time is more effective for the earth surface observation, the image quality is degraded by the three typical noises in azimuth and range directions. They are a periodic noise in the azimuth direction, which is so called the azimuth scalloping; the truncation noise in the azimuth direction, and the banding between the two scans, which appears in the range direction. SCANSAR scalloping is an artifact that is caused by the mismatching of the real azimuth power pattern and the optimum weighting function in the azimuth direction. Unless the noise floor level or the saturation at the SAR data is high enough, the correction of the scalloping is not difficult. The correction methods of the scalloping were proposed by several authors (Bamler???). They were to build the weighting function using the real azimuth antenna pattern and the multi looking intervals. They worked properly. In this paper, we proposed a method to estimate the azimuth weighting function using the Amazon forest, since the SAR data over the Amazon are uniform enough to determine the range antenna pattern. Second artifact is raised simply the signal truncation at the edge of the frequency spectrum. This will be easily solved by simply increase the pulse repetition frequency. However the parameter selection of the PRF and pulse burst numbers are sometimes limited by the SAR system. The third artifact as the banding between the scans is the problem but can be corrected in such a way that the SAR intensity is made continued and preserving the general range dependence of the intensity across the track.

ALOS PALSAR is under the operation from May 16 2006. The property of the PALSAR calibration is very stable (Shimada el al 2006). We applied this method to the PALSAR and confirmed the property of the three methods. In this paper, we will introduce the first two methods.

Keywords PALSAR, ALOS, Calibration and validation, Scalloping,

II SCALOPPING

1) Signal compression Model

When focusing on the same SCAN beam number, the time property of the range correlated and the SPECAN processed SCANSAR image can be expressed by the following equation.

$$P_r\left(T_{i,j}^k\right) = \frac{P_t G_a^2\left(T_{i,j}^k\right) G_r^2 \lambda^2}{(4\pi)^3 R^4}\sigma^0 + N_i^k \qquad (1)$$

$$T_{i,j}^k = i \cdot T_{SCAN} + j_k / f_{prf,k} \qquad (2)$$

$$T_{SCAN} = \sum_{i=0}^{N-1} \frac{n_{burst,i}}{f_{prf,i}} \qquad (3)$$

where, Pr the power of the SCANSAR image, Pt the transmission power, Ga the azimuth antenna pattern, Gr the range antenna pattern, λ the wave length, R the slant range, $\sigma 0$ the sigma-naught of the target, $T^k i,j$ is the azimuth time, and N the noise. i is the ith burst for kth scan, T_{SCAN} the period of all the scans, j the address in the burst, f_{prf} is the pulse repetition frequency. Here, the R^4 is due to that the time duration when the full deramp is applied is constant across the SCAN swath.

2) Multi looking in the time domain

Since time series of the SPECAN output (1) is truncated within the maximum burst number for each scan, the multi looking of the above signal data should be co-registered by shifting the data in time. The number of the multi looks is a function of the resolution and the sampling distance on the earth. The multi-looked power can be expressed by the followings;

$$\overline{P}_r(x) = \sum_{i \in n_{burst,j}} P_r(x)$$
$$x_i = \frac{v}{f_{prf}} \cdot i \qquad (4)$$

Periodic property of the function (4) depends on the azimuth antenna pattern Ga (x) and the Noise property. Here, x is the angular deviation from the center of the beam. Hereafter, we focus on the kth scan and thus the suffix k is omitted. If the SNR of the radar signal is quite low, the noise component in (4) can be ignored. The power deviation in the azimuth can be simply corrected by normalizing each power by azimuth antenna

ISBN: 978-4-88552-223-9 C3055©IEICE

pattern shifted with the time. Since the multi look processing reduces the noise component as 1/sqrt (N), the normalization can be given by

$$\overline{P}_r(x) = \frac{\sum_{i \in n_{burst,j}} P_r(x)}{\sum_{i \in n_{burst,j}} G_a(x)} \quad (5)$$

3) Weighting function

Weighting function is sometimes necessary for suppressing the signal bandwidth and side lobes. Unless the sampling frequency is big enough selected, weighting function is necessary accommodated. Out of the several functions, the Kaizer window is selected as its superior inband characteristics.

$$W_i = \frac{I_0\left(\pi\alpha\sqrt{1-(2k/n-1)^2}\right)}{I_0(\pi\alpha)} \quad 0 \le k \le n \quad (6)$$

where, I_D () is the first order Bessel function, α is the parameter for expressing the steepness of the in band characteristics, n is the width of the window.

4) Specan processing

The imaging can be done through the three steps, range correlation, range migration, and SPECAN processing, each of which is describes below,

(1) Range correlation:

$$g = f \oplus f_{r,ref} = F_r^{-1}\left(F_r(f) \cdot F_r\left(f_{r,ref}\right) \cdot W_r\right) \quad (7)$$

$$f_{r,ref} = \exp\left\{-2\pi j\left(\frac{k}{2}t^2\right)\right\} \quad (8)$$

where f the raw data, fr,ref the reference signal, Fr is Fourier transform in range, Wr is the window function in range, $\oplus$ is the correlation, and g the range correlated signal.

(2) Range migration

$$g' = F^{-1}\left(F_a(g) \cdot F_a(C) \cdot W_a\right) \quad (9)$$

where Fa is the Fourier transform in azimuth, C is the curvature in the range Doppler plane, Wa is the window function in azimuth, and g' is the range curvature signal.

(3) SPECAN

$$g'' = F_a^{-1}\left(g' \cdot f_{a,ref}\right) \quad (10)$$

$$f_{a,ref} = \exp\left\{-2\pi j\left(\frac{f_{DD}}{2}T^2 + f_D T\right)\right\} \quad (11)$$

where the fa, ref is the azimuth reference function, f_{DD} is the Doppler chirp, and f_D is the Doppler frequency, T is the time in azimuth direction, and g'' is the final output.

4) Azimuth antenna pattern

This pattern can be obtained by two ways. One is the direct measurement using the receiver, which is a part of the JAXA PARC (). The second method is deriving it from the SAR images. First method measures the one-way antenna pattern directly. Its Application to the real the processing routine needs the two-way path and the noise floor given by the SAR and processing routine. On the other hand, the second method automatically considers the noise level that the SAR is associated. Amazon rain forest is assessed as a group of the uniform scatterer and shows the constancy of the gamma-naught in the range direction. Thus, the area was often used as the determination of the SAR elevation antenna pattern (Shimada el al, 1995). We apply the same target as for the determination of the azimuth direction. Since the spectrum of the deramped range correlated signal shows the azimuth response of the target in considering the noise response. The average of the response gives the azimuth antenna gain, Ga, as

$$G_a(x) = \overline{g''}(x) \quad (12)$$

where, $\overline{g''}(x)$ shows the averaged output along the track. Thus the scalloping can be corrected by use of (12) at the averaging process of (5).

III. EXPERIMENTS

From this, we use the real data obtained by he PALSAR SCANSAR. First, the short description of the PALSAR CSANSAR is given below.

III-1. PSLSAR SCANSAR

PALSAR SCANSAR has two bands width of 14 MHz and 28 MHz. Those differ in the range resolution firstly, and are assigned to the difference mission. 14 MHz, whose mode is so called as WB1, is often used as the standard observation with the imaging swath of 350 km and look number for the averaging more than 3, while the 28 MHz band of SCANSAR, which is so-called as the WB2, is designed for the SCANSAR-SCANSAR interferometry operation. The latter one requires the synchronization of the IFOV on the earth. The specification of the SCANSAR modes is summarized in the Table 1. The number of looks is also shown in the Table 2. While there were four SARs appeared by now, the difference among is that the PLSAR has different pulse numbers and prfs. The palsar is designed to be operated up to 70 min. continuous operation. Because of the shorter antenna length of 8.9 meter and satellite height of 691.5 km, the prf changes 7 times and sampling window start time possibly varies at every 30 second. Thus, the processing of the SCANSAR for long path products needs the synchronization of the data among the different prfs. The ALOS is operated with yaw steering mode, and the Doppler frequency will be accommodated independent of the latitude.

Table 1 Characteristic of ALOS/PALSAR and SCANSAR

Item	Value
Height	691.5 km
Orbits	46 days recurrence and 671 orbits in total
Inclination	98.16 degrees

Orbit accuracy	10cm in average
Mass	4000Kg
Solar power	7000W at the beginning of life
Transmitter	80 TR modules for 2.0KW
Antenna size	8.9m in azimuth and 2.9m in range
Frequency	1270.0 MHz
Bandwidth	28.0 MHz (WB2), 14.0 MHz (WB1)
Sampling freq.	32.0 MHz (WB2), 16.0 MHz (WB1)
Pulse width	27.0 (μs)
Number of beams	3, 4, and 5
AD converters	I-Q, 5 bits
Swath width	350km at maximum
Gain control	MGC (Manual gain Mode)
Polarization	HH or VV

Table2 Look number distribution of PALSAR SCANSAR

No. scans	Long/short burst mode	Number of burst Number of looks
3	Short	247, 356, 274 6.54, 9.73, 7.42
4	Short	247, 356, 274, 355 4.82, 7.13, 5.44, 7.12
5	Short	247, 356, 274, 355, 327 3.6, 5.35, 4.08, 5.34, 5.03
3	Long	480, 698, 534 3.21, 3.94, 3.01
4	Long	480, 698, 534, 696 2.35, 2.89, 2.20, 2.82
5	Long	480, 698, 534, 696, 640 1.85, 2.27, 1.73, 2.21, 2.13

Note: all the burst number has zero data reception window of 12 to 13.

Table 3 Typical prfs (Hz) observed at WB1 5 SCAN

Scan No.	1	2	3	4	5
Hokkaido	1694	2375	1718	2164	1923
Amazon	1677	2352	1700	2141	1901
Louisiana	1686	2358	1709	2150	1912

Note: Doppler bandwidths for all the scans are 1700Hz

III-2. Weighting function

Weighted Azimuth antenna gain depends on the window function applied in (9). We show two patterns obtained by this calculation. One is obtained by using the rectangular window, and the second is obtained by the Kaiser window of a=0.7. Those pictures are shown in Fig. 1 and 2, respectively. X-axis is normalized by each burst number. The beam 1, 3 and 5 show small rise of the curve at the end. This means that the signal is truncated and detected at the end. This is due to a fact that the received signal is not fully sampled. The under sampling was measured. The best solution for these phenomena is to increase the sampling frequency. Although the PRF changes as a function of the time based on the satellite speed, which is measured in real time for monitoring the GPS receiver. The typical pattern of the PRF is shown in the table III. In general, #1, #3, and #5 beam has smaller PRF, while #2 and #4 has larger PRF. Thus, latter 2 beams are fully sampled. The Table 3 shows a typical prfs observed by short burst 5 scan WB1 over the Hokkaido, Japan on April 18 2006, Amazon, and the USA. The prfs for odd number beam is selected small, while the even numbered beam are selected large.

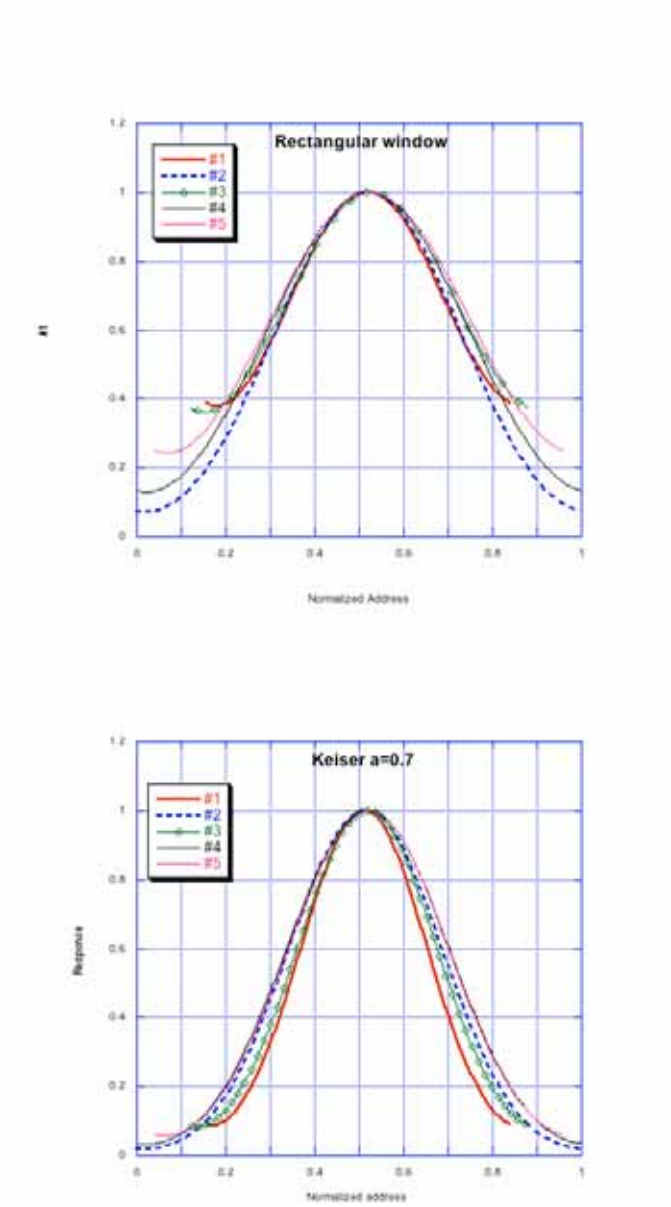

Fig. 1 Antenna gain pattern calculated from the Amazon data. a) Above with the rectangular window, and b) bottom with the Kaiser window (a=0.7).

III. Comparison of the Images generated by two windows

We generated two images using two weighting functions, and compared their image qualities. The selected targets are Amazon rain forest as the uniform target, and the coastal region of the Hokkaido, which is often interfered by the azimuth ambiguities.

III-1: Amazon case

As shown in Figures 2-a, and b. Both windows show the ideal responses and any irregularity cannot be observed. The power reduction due to the bandwidth suppression should be corrected at the NRCS calculation stage.

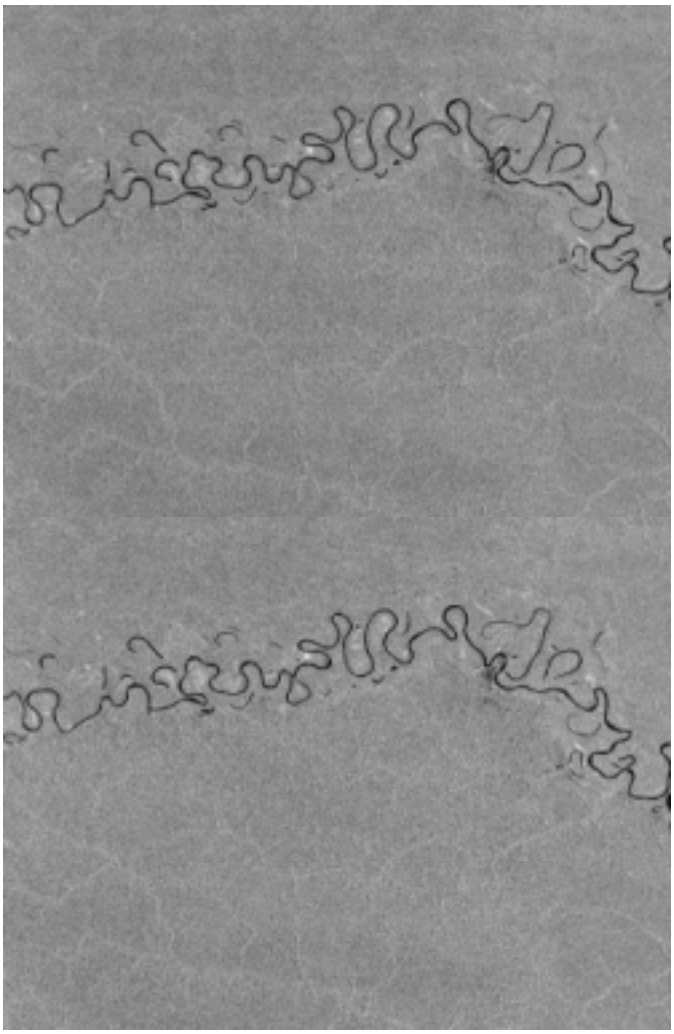

Fig. 2 SCANSAR image of the Amazon area, where the horizontal width has 130 km out of 350 km. The vertical striping, scalloping, cannot be seen.

III-2 Costal region at the Hokkaido

Image with the rectangular window remains the high ambiguity at the coastal region, especially at #3 and #5. This is due to the fact that the edge response of the smaller PRF is associated with the noise floor and the truncated signal at the higher spectrum causes the azimuth ambiguity. The image with the Kaiser window (Fig. 3-b) removes the azimuth ambiguity as #3 and #5 beams. This is due to that the weighting of the window suppress the signal truncation while the resolution in the azimuth direction is possibly reduced slightly.

IV. Conclusion

In this paper, we introduced a method for correcting the scalloping and suppressing the azimuth ambiguity in the SCANSAR image. The theory was shown and validated wit the experiments applied for the PALSAR SCANSAR data.

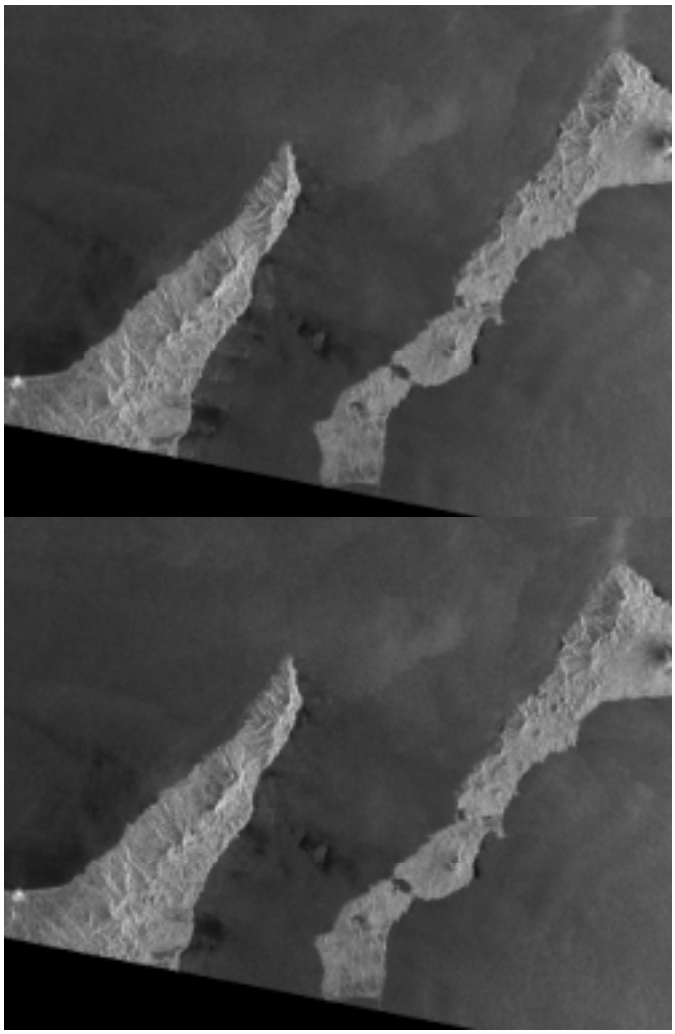

Fig. 3 SCANSAR image of the east of the Hokkaido, Japan, where the horizontal axis has 130km. The azimuth ambiguity south of the Shiretoko peninsula visible in above is corrected in the proposed windows and cannot be seen.

Acknowledgement

The authors express sincere thanks to Mr. Ito of JAXA ALOS, Kazuo Isono, and all the RESTEC PALSAR team members, and all the members of the JAXA ALOS PALSAR CAL/VAL and Science team members.

References

(1) Shimada M., N. Itoh, M. Watanabe, T. Moriyama, and T. Tadono, "PALSAR Initial Calibration and Validation Results ", Proc. of SPIE, Vol. 6359-6367, 11-16, Sept. 2006, Stockholm, Sweden.

(2)M. Shimada, and A. Freeman,"A technique for Measurement of Spaceborne SAR Antenna Patterns Using Distributed Targets," IEEE Trans. Geosci. Remote Sensing. Vol. 33, no. 1, pp. 100-114, January 1995.

(3) Bamler, R., "Optimum Look Weighting for Burst-Mode and ScanSAR Processing," IEEE Trans. Geosci. Remote Sensing. Vol. 33, no. 3, pp. 722-725, May 1995.